molecular pharmaceutics

Article

pubs.acs.org/molecularpharmaceutics

Mesoporous Silica Nanoparticles for Increasing the Oral Bioavailability and Permeation of Poorly Water Soluble Drugs

Yanzhuo Zhang,[†] Jiancheng Wang,[‡] Xiaoyu Bai,[‡] Tongying Jiang,[†] Qiang Zhang,*[,‡] and Siling Wang*[,†]

[†]Department of Pharmaceutics, School of Pharmacy, Shenyang Pharmaceutical University, Wenhua Road 103, Shenyang 110016, P. R. China

[‡]State Key Laboratory of Natural and Biomimetic Drugs, School of Pharmaceutical Sciences, Peking University, Beijing, 100191, P. R. China

ABSTRACT: We investigate the effects of spherical mesoporous silica nanoparticles (MSNs) as an oral drug delivery system to improve the oral bioavailability of the model drug telmisartan (TEL) and examine their cellular uptake and cytotoxicity. Further, we explore the mechanisms behind the improved oral absorption of poorly soluble drugs promoted by MSNs. An investigation of intestinal epithelial cellular binding, association and uptake was carried out by laser scanning confocal microscopy, transmission electron microscopy and fluorescence activated cell sorting. The results show that the cellular uptake is highly time-, concentration- and size-dependent. The model drug permeability studies in the human colon carcinoma (Caco-2) cell lines indicated that MSNs could significantly enhance TEL permeability and reduce rate of drug efflux. After loading TEL into MSNs, its oral bioavailability was compared with that of the marketed product Micardis and TEL-loaded ordered mesoporous silica microparticles (MSMs) in beagle dogs. The relative bioavailability of TEL-loaded MSN formulation and TEL-loaded MSM formulation was 154.4 ± 28.4% and 129.1 ± 15.6%, respectively. MSNs offer the potential to achieve enhanced oral bioavailability of poorly soluble drugs via improved drug dissolution rate and enhanced drug permeability.

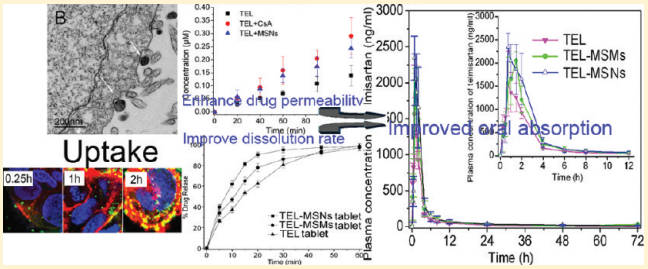

KEYWORDS: *drug delivery, mesoporous, nanoparticles, cellular uptake, permeability, bioavailability*

INTRODUCTION

Oral delivery is the most preferred route for the administration of drug formulations due to its simplicity.[1] However, it is estimated that 40% of new chemical entities (NCE) are poorly soluble or insoluble in water.[1,2] Dissolution rate in gastrointestinal fluids (GI) and permeability through biological membranes are considered as the most important aspects in determining the bioavailability of orally administered poorly soluble drugs.[3−5] Nanotechnology has benefited a number of biomedical areas including drug delivery.[6,7] The use of nanostructured materials (e.g., nanoparticles) as drug delivery systems has begun to impact biomedical areas due to beneficial size-dependent physical and chemical properties.[8−12] In the past decade, mesoporous materials (pore diameter 2−50 nm) have found widespread application as controlled drug delivery systems.[13−15] Mesoporous materials offer several attractive features for controlled release, such as a high adsorption capacity,[16,17] the ability of the mesoporous channels to change the crystalline state of a drug to an amorphous one,[18−20] the possibility of stabilizing loaded drugs within these pores and the ease of modifying the pore dimensions to control drug delivery kinetics.[21,22]

In previous studies, mesoporous materials have been mainly used to develop slow-release formulations, and a few model drugs, such as ibuprofen,[20,23] griseofulvin,[24] nimodipine,[25] carbamazepine,[26] itraconazole[27] and simvastatin,[28] have been loaded into mesoporous materials and investigated *in vitro*. When the release of the model drugs from mesoporous materials was examined *in vitro*, it was found that sustained release took place which was dependent on the pore size, morphology and the pore channel length of the mesoporous materials used.[29,30] However, few *in vivo* studies have been conducted using drug delivery systems involving mesoporous silica nanoparticles (MSNs) and, as far as we are aware, there are no reports of the use of spherical MSNs (particle diameter less than 100 nm) for oral drug delivery *in vivo* and no reports of the determination of their intestinal epithelial cellular uptake as well as investigation of their effects on drug permeability.

The aim of this work was to investigate the effects of MSNs as an oral drug delivery system on the oral bioavailability and permeability of the model drug TEL. In addition, it is important to determine their cellular uptake and cytotoxicity for future applications. To achieve this aim, the oral bioavailability of TEL-loaded MSNs was compared with that of the commercial product Micardis and TEL-loaded MSMs in beagle dogs, the model drug permeability studies using the Caco-2 cell monolayers. A systematic evaluation of the intestinal epithelial

Received: June 4, 2011
Revised: December 25, 2011
Accepted: January 4, 2012
Published: January 4, 2012

cellular binding, association and uptake was carried out using transmission electron microscopy (TEM), fluorescene-activated cell sorting (FACS) and laser scanning confocal microscopy (LSCM).

EXPERIMENTAL SECTION

Cell Lines and Drugs. Human colon carcinoma (Caco-2) cell lines were obtained from American Type Culture Collection (ATCC, Manassas, VA, USA) and used at passages 40−60. Telmisartan (TEL, 98.0%) was purchased from Sigma-Aldrich (St. Louis, MO, USA) and used as received. Valsartan (99%) was obtained from the National Institute for the Control of Pharmaceutical and Biological Products (Beijing, China). Telmisartan tablets (Micardis) were purchased from Boehringer Ingelheim Pharma GmbH (Ingelheim am Rhein, Germany).

Chemicals. Hoechst 33258, rhodamine-phalloidin, Pluronic 123 triblock polymer $[(EO)_{20}(PO)_{70}(EO)_{20}]$, thiazolyl blue tetrazolium bromide (MTT), defined fetal bovine serum (FBS), guaranteed-grade glucose, nonessential amino acids, L-glutamine, penicillin streptomycin, trypsin, bovine serum albumin and Dulbecco's modified Eagle's medium (DMEM) were purchased from Sigma-Aldrich (St. Louis, MO, USA). HPLC-grade methanol, acetonitrile and phosphoric acid were purchased from Merck (Darmstadt, Germany). Guaranteed-grade 3-aminopropyltriethoxysilane (APTES), tetraethyl orthosilicate (TEOS), 1,3,5-trimethylbenzene (TMB) and fluorescein isothiocyanate isomer (FITC) were purchased from Aladdin (Shanghai, China). All other chemicals were of reagent grade and used as purchased without further purification.

Synthesis of FITC-MSNs, MSMs and FITC-MSMs. Spherical MSNs and APTES modified MSNs (AP-MSNs) were synthesized according to the procedure reported by Zhang et al.[31] For fluorescence detection, MSNs were matrix-labeled with the fluorescent dye FITC. Briefly, 200 mg of AP-MSNs was resuspended in 10 mL of carbonate buffer solution (pH 9.0). Then AP-MSNs were mixed with 1 mg/mL FITC solution. The suspension was stirred at 4 °C for 10 h, and the FITC labeled MSNs were collected by centrifugation (at 12,000 rpm). After thorough washing of the labeled materials with carbonate buffer, the particles were dried under vacuum and stored as dry powders. The dried composite samples were named FITC-MSNs.

Fibrous MSMs were synthesized according to the procedure reported by Zhao et al.[32] with some modifications. The preparation, in brief, was as follows: 2.0 g of Pluronic 123 triblock copolymer was dissolved in a mixture of 15 mL of water and 60 mL of 2 M hydrochloric acid solution; then, 0.025 g of ammonia tetrafluoride and 0.75 mL of TMB were added to the surfactant solution, the mixture was stirred for 2 h, and 4.5 mL of TEOS was added to the solution. Following this, the reaction solution was stirred for 24 h at 38 °C and the mixed solution was then allowed to stand at 120 °C for 24 h. The solid product was filtered, dried in air, and calcined at 600 °C for 5 h. The procedure for FITC labeling of MSMs was similar to that used for labeling MSNs, and the dried composite samples were named FITC-MSMs.

Drug Encapsulation and *in Vitro* Dissolution Tests. *Preparation of TEL-Loaded MSNs.* The procedure for loading TEL into MSMs was similar to that used for loading MSNs.[31] Briefly, MSMs were transferred into an acetic acid solution of TEL (100 mg/mL). The MSMs:TEL ratio in the loading solution was 5:3 (w:w). Then, the mixture was ultrasonicated, vortexed under ambient conditions and dried. The dried composite samples were named TEL-MSMs. The TEL-MSNs tablets were prepared by a process of direct compression with physically blending TEL-MSNs, mannitol, microcrystalline cellulose and cross-linked polyvinylpyrrolidone (in a mass ratio of 35/25/25/15).

Field Emission Scanning Electron Microscopy (FESEM), Field Emission Transmission Electron Microscopy (FETEM) and Nitrogen Adsorption Studies. The morphology and particle size of the prepared samples were characterized using a JSM-6301F FESEM instrument (JEOL, Japan). The porous structure of the samples was characterized using a Tecnai G2 F30 FETEM instrument (FEI, The Netherlands). Before examination, the samples were dispersed in deionized water through sonication and subsequently deposited on carbon-coated copper grids. The pore characteristics of the samples were studied by determining the nitrogen adsorption using a SA3100 surface area and pore size analyzer (Beckman Coulter, USA) at −196 °C. The MSNs (or SBA-15) samples were degassed at 300 °C for 12 h prior to analysis, while the TEL-loaded samples were degassed at 50 °C for 12 h.

In Vitro Dissolution Study. The *in vitro* dissolution study was conducted using a USP II paddle method with a D-800 LS dissolution tester (Tianjin University Radio Factory, China). TEL-loaded tablet samples, equivalent to 40 mg of TEL, were exposed to enzyme-free simulated intestinal fluid (pH 6.8).[33] At predetermined intervals, 5 mL samples were withdrawn and suitably diluted and then the drug concentration was determined by a HPLC system consisted of a L7100 pump and a L7420 UV−vis tunable absorbance detector (Hitachi, Japan). Analysis was carried out on a reversed-phase C_{18} column (Agilent Zorbax Rx, 5 μm, 4.6 × 250 mm). The mobile phase consisted of an 80:20 (%v/v) mixture of methanol and 5 mM potassium dihydrogen phosphate solution, the flow rate was 1.0 mL/min and the detection wavelength was 296 nm.

Uptake and Cytotoxicity in Caco-2 Cell Experiments. *Laser Scanning Confocal Microscopy (LSCM) Study.* For LSCM measurements, Caco-2 cells were seeded at a density of 5×10^4 cells per well in 12-well plates in 1 mL of DMEM medium with coverslips at the bottom of the wells and allowed to attach and proliferate for 7 days until reaching a confluence of 80−90%. The culture medium was changed three times a week. Afterward, adherent cells were incubated with 50 μg/mL FITC-MSNs (or FITC-MSMs) in the serum-free DMEM medium for various incubation times. The Caco-2 cells were washed three times with PBS and then fixed in 4% formaldehyde solution in PBS at room temperature for 10 min. The cells were then washed twice with PBS and incubated with 0.1% Triton X-100 plus 1% bovine serum albumin in PBS at room temperature for 30 min followed by 1 μg/mL Hoechst 33258 staining in PBS for 20 min. The Caco-2 cells were then washed twice with Hanks balanced salt solution (HBSS), followed by Rhodamine-phalloidin staining in PBS for 20 min. After staining, fixed cells were examined under a TCS NT Sp5 LSCM instrument (Leica, Germany) using a 63× oil immersion objective.

Transmission Electron Microscopy (TEM) Study. For TEM measurements, Caco-2 cells were seeded at a density of 5×10^4 cells per well in 6-well plates over a week. The culture was maintained under standard culture conditions at a temperature of 37 °C and in a humidified atmosphere of 5% CO_2. The medium was then removed, and 100 μL of MSN suspensions

(100 μg/mL in the serum-free DMEM) were added to each well and incubated for 4 h. After incubation, the medium containing the MSNs not taken up by the cells was discarded, and the cells were washed twice with PBS. Cells were collected from the 6-well plates and centrifuged at 1000*g* for 5 min, and the supernatant was removed. The cell pellets were fixed with 2% glutaraldehyde in 0.1 M PBS solution (pH 7.4) for 10 h at 4 °C. Afterward, the cells were rinsed with 0.1 M PBS, embedded in 2% agarose gel, and postfixed in 4% osmium tetroxide solution. The cells were then dehydrated and embedded in epoxy resin. The resin was polymerized at 60 °C for 24 h. Ultrathin sections (50−70 nm) obtained with an ultramicrotome (EMUC6, Leica, Germany) were poststained with 5% aqueous uranyl acetate and 2% aqueous lead citrate and examined with a H9000 TEM instrument (Hitachi, Japan).

Fluorescene Activated Cell Sorting (FACS) Study. For the flow cytometry assays, Caco-2 cells were seeded at a density of 1×10^5 cells per well in 6-well plates in 1 mL of DMEM medium and allowed to attach and proliferate for 7 days until reaching a confluence of 60−70%. The media were then removed from the wells, and the attached cells were washed with PBS. Afterward, adherent cells were incubated with different concentrations of FITC-MSNs in the serum-free DMEM medium for various incubation times. Treated Caco-2 cells were washed three times with PBS and then harvested by trypsinization. Caco-2 cells without any addition of nanoparticles (the serum-free DMEM treated cells) were carried along as a control in every measurement. After centrifugation the cell pellets were resuspended in PBS containing 0.1% FBS. All the tests were run in triplicate. The cellular uptake of FITC-MSNs was determined by a FACS instrument (Becton Dickinson, CA).

In Vitro Cytotoxicity Assay. For cytotoxicity assay, Caco-2 cells were seeded at a density of 5×10^3 cells per well in 96-well plates over a week. Caco-2 cells were incubated with different concentrations of MSNs in the serum-free DMEM medium for various incubation times. Caco-2 cells cultured in the absence of MSNs acted as controls. The MTT reagent was subsequently added for a further 24 h. Cytotoxicity was determined by measuring the reduction of the yellow tetrazolium salt MTT to water-insoluble purple formazan crystals by metabolic active cells. Then, 100 μL of DMSO was added to each well and left in the dark at room temperature for 24 h. The absorbance of the resulting formazan solution was recorded at 590 nm with an Infinite M200 microplate reader (Tecan, Germany).

Caco-2 Permeability Experiments. Caco-2 cells (5×10^5 cells) were seeded onto Transwell polycarbonate inserts and grown for 21−28 days, renewing the culture medium every other day. The cells were left to differentiate for 15−21 days after being seeded, and then transepithelial electrical resistance (TEER) values monitored using a Millicell ERS meter (Millipore, Bedford, MA, USA) should be more than 500 Ω/cm^2. Prior to the experiment, the cells were washed with HBSS pH 7.4 buffer (with 10 mM HEPES) and incubated with HBSS pH 7.4 buffer for 1 h. For an apical (AP) to basolateral (BL) permeation direction (AP → BL) study, 1.5 mL of HBSS was added to the basolateral side and 0.5 mL of test solution was added to the apical side. For the basolateral to apical permeation direction (BL → AP) study, 0.5 mL of HBSS was added to the apical side and 1.5 mL of test solution was added to the basolateral side. Following addition of the different test solution (2 μg/mL TEL solution, 2 μg/mL TEL solution with 12 μg/mL cyclosporin A and 2 μg/mL TEL solution with 75 μg/mL MSNs, respectively.), the plates were incubated at 37 °C, 5% CO_2, 95% humidity, and shaking at 50 rpm. At predetermined intervals, 100 μL samples were drawn out of the acceptor compartment and immediately replaced with an equal volume of HBSS medium to keep the volume constant. Sample was stored at −20 °C until HPLC analysis. Results were expressed as cumulative transport as a function of time. All experiments were done in triplicate. The apparent permeability coefficient (P_{app}) was calculated according to eq 1,

$$P_{app} = (dQ/dt)/(A \times C_0)\ \text{cm}\cdot\text{s}^{-1} \quad (1)$$

where dQ/dt (mol/s) is the permeability rate of TEL on the acceptor compartment, A is the effective growth area of the monolayers (1.12 cm^2), and C_0 (mol/L) is the initial drug concentration in the donor compartment.

Absorption enhancement ratios (AR) were calculated according to eq 2:

$$AR = P_{app(AP\rightarrow BLsample)}/P_{app(AP\rightarrow BLcontrol)} \quad (2)$$

Efflux ratios (ER) were calculated from P_{app} values by using eq 3:

$$ER = P_{app(BL\rightarrow AP)}/P_{app(AP\rightarrow BL)} \quad (3)$$

***In Vivo* Absorption Studies.** *Animal Experiments.* All the procedures used in the present study were conducted according to the guidelines approved by the Institutional Animal Care and Ethical Committee of Shenyang Pharmaceutical University. Six male beagle dogs, weighing 10−12 kg, were randomly allocated to three treatment groups and given tablets based on MSNs loaded with TEL, tablets based on MSMs loaded with TEL, and the commercial tablets (Micardis) according to a three-period crossover experimental design. A wash-out period of 7 days was allowed between dose administrations. The dogs were fasted for 12 h prior to the experiments but were allowed free access to water. Each dose (40 mg, expressed as TEL equivalents) was given by gavage. After receiving the oral dose, 20 mL of water was given to facilitate swallowing. After 4 h, the dogs had free access to food and water. Blood samples (1.5 mL) were taken from the vena jugularis before drug administration and at 0.25, 0.5, 0.75,1, 1.5, 2, 4, 6, 8, 12, 24, 48, and 72 h. These blood samples were collected in heparinized tubes and centrifuged for 15 min at 4000 rpm, and the plasma obtained was stored at −20 °C until HPLC analysis.

Bioanalytical Method. Plasma concentrations of TEL were determined by an isocratic HPLC method. After addition of 50 μL of internal standard solution (valsartan, 100 μg/mL in methanol) to 0.4 mL of plasma, 1.5 mL of acetonitrile was added. Plasma proteins were precipitated by vortex mixing for 3 min. Following centrifugation at 9000 rpm for 10 min, the upper organic layer was removed and a 20 μL aliquot was injected into the HPLC system. The HPLC system (Hitachi, Japan) consisted of two L2130 pumps, an L2000 Elite chromatography system controller, an L2300 column oven and an L2485 fluorescence detector. The data were collected and processed using L2000 Elite chromatography data station software. The HPLC separation was performed using a reversed-phase C_{18} column (Agilent Zorbax Rx, 5 μm, 4.6 × 250 mm). The oven temperature was set at 40 °C, and the mobile phase consisted of methanol−10 mM potassium dihydrogen phosphate solution (adjusted to pH 3.0 with phosphoric acid)−acetonitrile in a volume ratio of 20/45/35

(v/v/v) which was eluted at a flow rate of 1.5 mL/min. The fluorescence detection was performed at an excitation wavelength of 300 nm and an emission wavelength of 385 nm. The analyses were identified from the retention times of 98−99% pure reference standards. Under these chromatographic conditions, the retention time was 6.7 min for telmisartan and 5.4 min for valsartan. Calibration curves (2−200 ng/mL, seven different concentrations) and QC samples (2, 50, and 150 ng/mL) were prepared freshly for each analysis. The linear regression coefficients of the calibration curves ranged from 0.9991 to 0.9997. The lower limit of quantification and detection for this analytical method were 1 and 0.5 ng/mL, respectively. The accuracy and the precision of the QC samples ranged from 95.2 to 104.6% of the nominal values, with a CV (coefficient of variation) of 2.5 to 7.3%, respectively. The absolute recovery of TEL from the QC samples (n = 9) was 90.1 ± 2.4%.

Pharmacokinetic Calculations. The pharmacokinetic parameters were determined using the PC software of the Drug and Statistics (DAS version 2.1.1) computer program (issued by the State Food and Drug Administration of China for pharmacokinetic study), employing a noncompartmental model. The maximum plasma concentration (C_{max}) and the time to reach the C_{max} (t_{max}) were obtained from the individual subject plasma concentration versus time curves. The relative bioavailability (F_r) was calculated using the following eq 4:

$$F_r(\%) = [\mathrm{AUC}_{0\rightarrow t(\mathrm{test})}/\mathrm{AUC}_{0\rightarrow t(\mathrm{reference})}] \times 100 \quad (4)$$

where $\mathrm{AUC}_{0\rightarrow t(\mathrm{reference})}$ is the $\mathrm{AUC}_{0\rightarrow t}$ after oral administration of Micardis, while $\mathrm{AUC}_{0\rightarrow t(\mathrm{test})}$ represents that of the formulation based on MSNs (or SBA-15) loaded with TEL.

Statistical Analysis. The experimental data were analyzed using the Statistical Package for Social Sciences (SPSS version 11.0). Post hoc multiple comparisons were performed using one-way analysis of variance (ANOVA) and the Student−Newman−Keuls test to determine the significance of differences between groups. The difference was considered to be statistically significant if the probability value was less than 0.05 ($p < 0.05$).

RESULTS AND DISCUSSION

Solid State Characterization. FESEM imaging showed that the MSM sample consisted of many rodlike subparticles with a relatively uniform size of about 0.5 μm in diameter and 1−2 μm in length, which were aggregated into wheatlike macrostructures (Figure 1A). As shown in Figure 1B, the FETEM image confirms the ordered mesoporous structure of MSMs. The pore diameter of SBA-15 was approximately 12 nm. As shown in Figures 1C and 1D, FITC-MSNs and FITC-MSMs retained the shape of the MSNs and MSMs, respectively. The values for the BET specific surface area, the total pore volume and the BJH pore diameter of MSMs were 917.6 m^2/g, 1.15 cm^3/g and 11.3 nm, respectively.

***In Vitro* Dissolution.** The effect of the prepared TEL-loaded MSN (or MSM) formulation on the TEL dissolution rate in enzyme-free simulated intestinal fluid (pH 6.8) is shown in Figure 2. The dissolution rate of TEL from a TEL-loaded MSN tablet or TEL-loaded MSM tablet was significantly improved. The dissolution improvement may be largely attributed to the pore channels of the two carriers changing the crystalline state of TEL to an amorphous state, which is known to improve the drug solubility and dissolution rate. In addition, the particle sizes of the amorphous drug incorporated in the pore channels (nanometer range) were significantly reduced compared with that of pure crystalline TEL (micrometer range). It is evident that a further decrease in the particle size down to the nanometer range will further accelerate the drug release profile and, consequently, improve the dissolution rate.[2,8,24] It is worth noting that a faster TEL release of the two drug-loaded samples was observed from the TEL-loaded MSN tablet. The difference in release rate between the TEL-loaded MSN tablet and the TEL-loaded MSM tablet could be attributed to the carrier pore channel length. The TEL molecules adsorbed in the short MSN pore channels (the pore channel length was less than the radius of MSN) have a greater chance of escaping from the pore channels and diffusing into the release medium compared with those adsorbed in the 2-D cylindrical MSM pore systems (the pore channel length was more than 1 μm, as shown in Figures 1A and 1C).

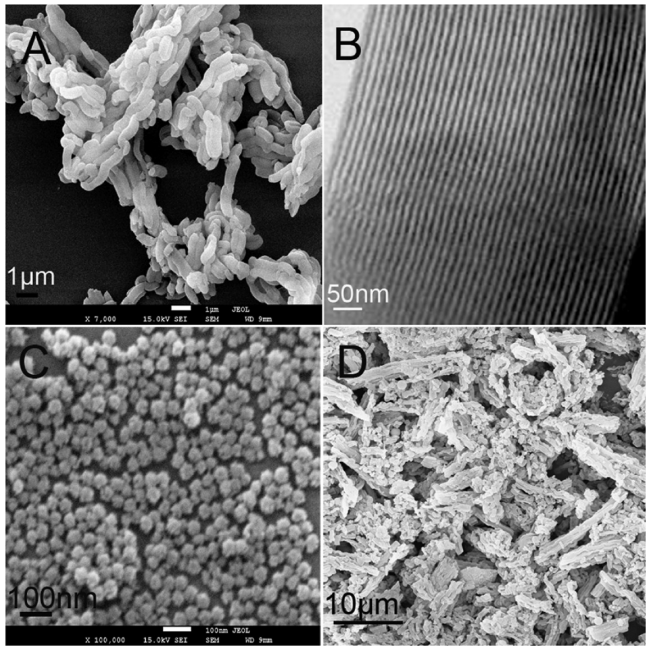

Figure 1. FESEM photographs of (A) MSMs, (C) FITC-MSNs and (D) FITC-MSMs. FETEM photograph of (B) MSMs.

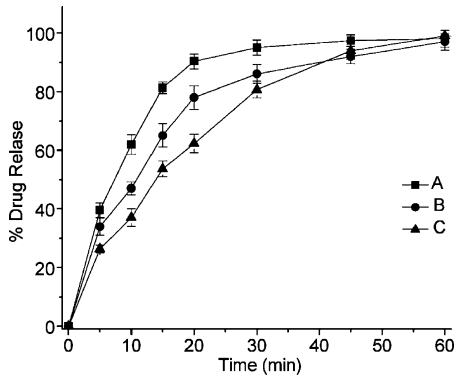

Figure 2. Dissolution profiles of TEL from (A) TEL-loaded MSN tablet, (B) TEL-loaded MSM tablet and (C) TEL commercial tablet in PBS (pH6.8). Each data point represents the mean ± SD of three determinations.

Uptake and Cytotoxicity in Caco-2 Cells. *Laser Scanning Confocal Microscopy (LSCM).* The cellular binding,

dx.doi.org/10.1021/mp200287c | *Mol. Pharmaceutics* 2012, 9, 505−513

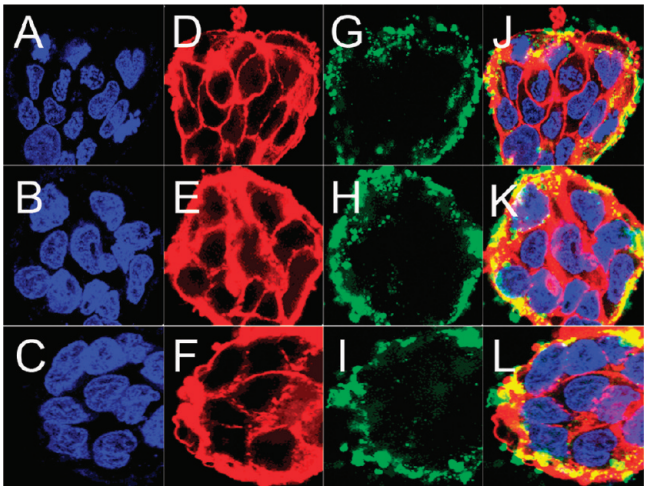

Figure 3. Confocal microscopy images of Caco-2 cells after 1 h incubation at 37 °C with FITC-MSN [MSNs with sizes of about 20 nm (A, D, G, J), 60 nm (B, E, H, K), 90 nm (C, F, I, L)] particles: fluorescent images of the cell nucleus (A–C), fluorescent images of the plasma membrane (D–F), images of FITC-MSN fluorescence in cells (G–I), image of FITC-MSN fluorescence superimposed on the nucleus and plasma membrane (J–L). The fluorescence detection of FITC was performed at an excitation wavelength of 490 nm and an emission wavelength of 520 nm. The fluorescence detection of Hoechst 33258 was performed at an excitation wavelength of 360 nm and an emission wavelength of 440 nm. The fluorescence detection of Rhodamine-phalloidin was performed at an excitation wavelength of 485 nm and an emission wavelength of 595 nm.

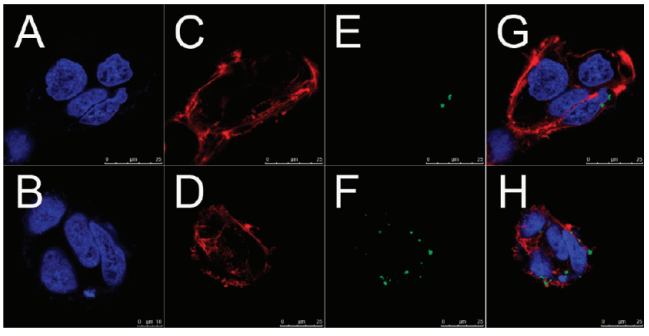

Figure 4. Confocal microscopy images of Caco-2 cells after 0.25 h (A, C, E, G) or 2 h (B, D, F, H) incubation at 37 °C with FITC-MSM particles: fluorescent images of the cell nucleus (A, B), fluorescent images of the plasma membrane (C, D), images of FITC-MSM fluorescence in cells (E, F), image of FITC-MSM fluorescence superimposed on the nucleus and plasma membrane (G, H).

association and transport of FITC-MSNs were examined by LSCM. Merged LSCM images of Caco-2 cells show that FITC-MSNs with different sizes of about 20, 60, and 90 nm were internalized into Caco-2 cells after 1 h incubation at 37 °C, as shown in Figure 3. Inside the Caco-2 cells, FITC-MSNs formed nonuniform green fluorescent aggregates and mostly accumulated in the cell membrane region, but did not penetrate the nucleus. In contrast, no FITC-MSMs produced a green fluorescence inside the Caco-2 cells, as confirmed by measurement of their particle size (Figure 4). As shown in Figure 5, Caco-2 cells were incubated with 50 μg/mL FITC-MSNs (with sizes of about 90 nm) in serum-free DMEM medium for various incubation times. The results show that cellular uptake is highly time-dependent. LSCM images showed

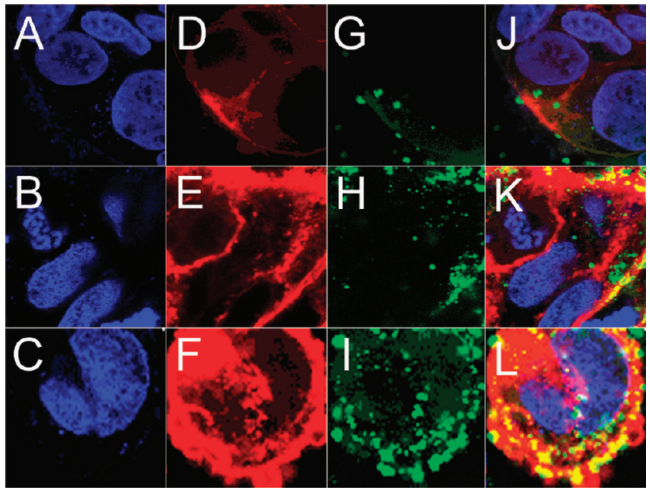

Figure 5. Confocal microscopy images of Caco-2 cells after 0.25 h (A, D, G, J), 1 h (B, E, H, K) or 2 h (C, F, I, L) incubation at 37 °C with FITC-MSN particles: fluorescent images of the cell nucleus (A–C), fluorescent images of the plasma membrane (D–F), images of FITC-MSN fluorescence in cells (G–I), image of FITC-MSN fluorescence superimposed on the nucleus and plasma membrane (J–L).

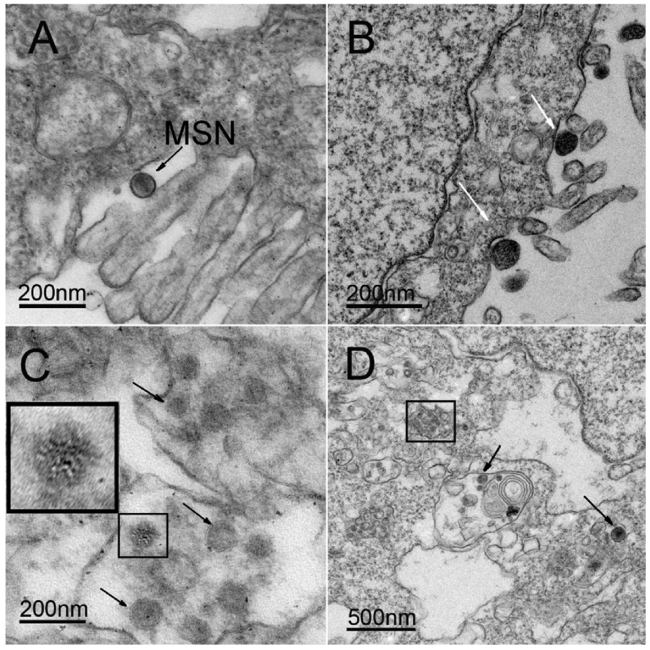

Figure 6. TEM photographs of the cellular uptake of MSNs.

that FITC-MSNs were internalized into Caco-2 cells after 0.25 h incubation at 37 °C. Interestingly, FITC-MSNs remained mainly in the cytoplasm, but did not penetrate the nucleus after a 2 h incubation at 37 °C (the intracellular distribution of MSNs in the Caco-2 cells will be further examined by TEM).

Transmission Electron Microscopy (TEM). We further evaluated the possible mechanisms of cellular uptake of MSNs by TEM. Literature reports suggest that the uptake of nanoparticulate systems into cells can typically occur through several different processes, such as nonspecific diffusion, phagocytosis and endocytosis.[19,34,35] Figure 6 shows the endocytosis of MSNs by Caco-2 cells. As shown in Figure 6A, an MSN particle binds to the intestinal villi. As shown in Figure 6B, few MSNs bound to the cell membrane and an MSN

dx.doi.org/10.1021/mp200287c | *Mol. Pharmaceutics* 2012, 9, 505–513

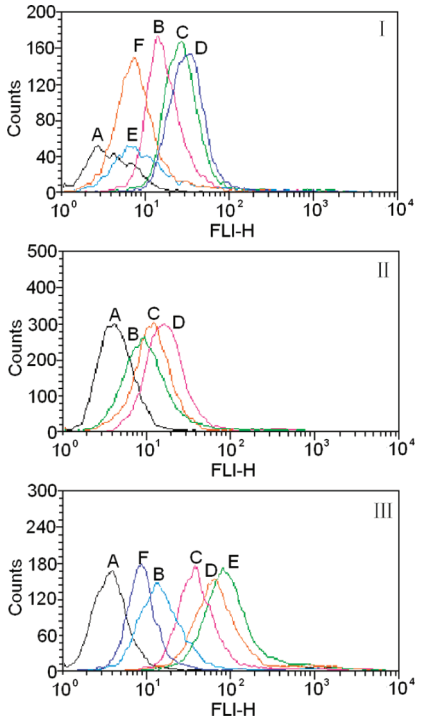

Figure 7. (I) Fluorescent intensity of control Caco-2 cells (A), Caco-2 cells after a 0.5 h (B), 1 h (C) or 2 h (D) incubation at 37 °C with FITC-MSN particles and Caco-2 cells after a 0.5 h (E) or 2 h (F) incubation at 37 °C with FITC-MSMs. (II) Fluorescent intensity of control Caco-2 cells (A), Caco-2 cells incubation at 37 °C with FITC-MSNs with sizes of about 90 nm (B), 60 nm (C) and 20 nm (D). (III) Fluorescent intensity of control Caco-2 cells (A), Caco-2 cells after 2 h incubation with FITC-MSNs at concentrations of 20 μg/mL (B), 100 μg/mL (C), 200 μg/mL (D), 250 μg/mL (E) and Caco-2 cells after 2 h incubation with FITC-MSMs at a concentration of 250 μg/mL (F).

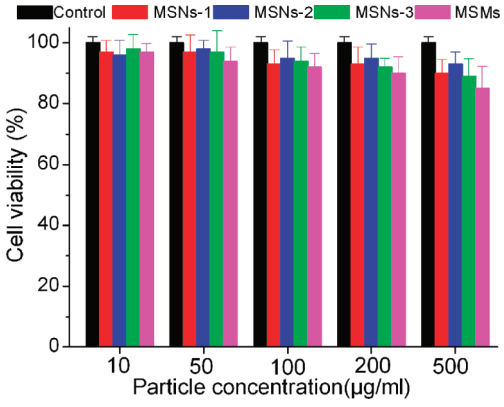

Figure 8. Effect of MSNs with different sizes and MSMs on the Caco-2 cell viability at various concentrations from 10 μg/mL to 500 μg/mL.

entered through the cell membrane. As shown in Figures 6C and 6D, most of the internalized MSNs accumulate in the vesicular or cytosolic compartment inside Caco-2 cells as confirmed by measurement of their particle size and mesostructure. These results provide visual evidence of the cellular uptake of MSNs. From the TEM images, we can hypothesize that the process of MSN internalization is as follows: first, MSNs are bound to the intestinal villi or cell membrane. Then, MSNs are internalized in Caco-2 cells by nonspecific cellular uptake and merge with endosomes.

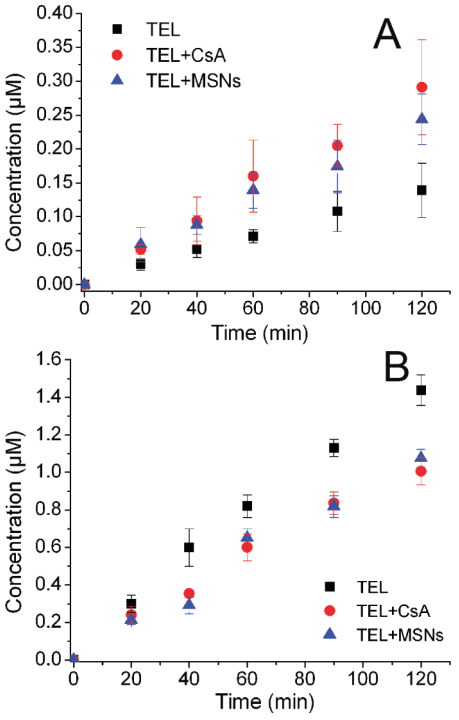

Figure 9. The mean cumulative transport versus time curves of 3.88 μmol/L TEL in the directions of (A) AP → BL and (B) BL → AP in Caco-2 cell monolayer. Each data point represents the mean ± SD (n = 3). *Significant difference ($p < 0.05$) compared with the control group (TEL group).

Table 1. Mean P_{app} of Telmisartan (TEL) in the Directions of AP → BL and BL → AP Sides

samples	$P_{app(AP\rightarrow BL)} \times 10^6$ (cm·s^{-1})	$P_{app(BL\rightarrow AP)} \times 10^6$ (cm·s^{-1})	efflux ratio
TEL	6.27 ± 1.09	21.44 ± 1.13	3.47 ± 0.43
TEL + CsA	13.11 ± 2.85[a]	16.08 ± 0.95[a]	1.25 ± 0.20[a]
TEL + MSNs	10.86 ± 2.26[a]	17.22 ± 0.82[a]	1. 62 ± 0.28[a]

[a]Significant difference ($p < 0.05$) compared with the control group (TEL group).

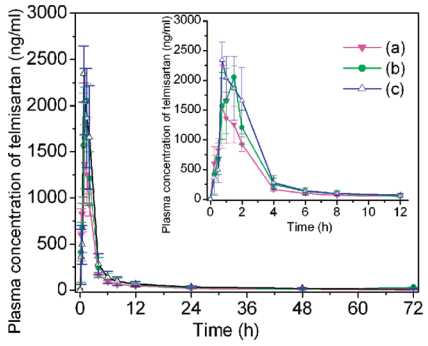

Figure 10. The mean plasma concentration versus time curves of TEL following an oral dose of (a) a Micardis tablet, (b) a TEL-MSM tablet and (c) a TEL-MSN tablet (equivalent to 40 mg of TEL) in beagle dogs. Each data point represents the mean ± SD (n = 6).

Subsequently MSNs escape from the endosomes and enter the cytoplasm. In contrast, the fibrous MSMs incubated with the Caco-2 cells were not internalized nor were they visible in any of the ultrathin sections by TEM, which further supports

dx.doi.org/10.1021/mp200287c | Mol. Pharmaceutics 2012, 9, 505–513

Table 2. Mean and Standard Deviation Values of the Pharmacokinetic Parameters of Telmisartan (TEL) Formulations after Oral Administration to Beagle Dogs (n = 6)

formulation	t_{max} (h)	C_{max} (ng/mL)	$t_{1/2}$ (h)	$AUC_{0\rightarrow 72h}$ (ng·h/ml)	$AUC_{0\rightarrow\infty}$ (ng·h/ml)	rel bioavailability[a] (%)
TEL-MSN tablet	0.96 ± 0.29[c]	2315.17 ± 150.20[b]	22.07 ± 9.10	7432.70 ± 1491.56[b,c]	7770.43 ± 1318.82[b,c]	154.4 ± 28.4
TEL-MSM tablet	1.42 ± 0.2[b]	2102.4 ± 253	22.75 ± 13.19	6183. 69 ± 671. 68[b]	6487.36 ± 683.42[b]	129.1 ± 15.6
commercial tablet	1 ± 0.27	1891.65 ± 272.81	18.73 ± 4.51	4804.26 ± 306	4930.77 ± 381.77	

[a]Calculated based on $AUC_{0\rightarrow t}$ with the commercial tablet as reference. [b]Significant difference ($p < 0.05$) compared with the commercial tablet. [c]Significant difference ($p < 0.05$) compared with TEL-MSM tablet.

the observed images by LSCM due to their wheatlike macrostructures.

Fluorescene Activated Cell Sorting (FACS). The cellular association of the particles was also investigated via FACS. As shown in Figure 7A, control cells which were not incubated with nanoparticles always emitted weak background fluorescence. In contrast, cells which were associated with fluorescently labeled particles exhibited higher fluorescence intensity. These results show that cellular uptake is highly time- and size-dependent (Figures 7I and 7II). The uptake of FITC-MSNs (100 μg/mL) after a 2 h incubation was approximately 1.4 times that of FITC-MSNs after 1 h incubation, and 2.3 times that of FITC-MSNs after a 0.5 h incubation. In contrast, the uptake of FITC-MSMs (100 μg/mL) after a 2 h incubation was less than that of FITC-MSNs (100 μg/mL) after a 0.5 h incubation, which also confirms the results obtained from the LSCM study. Cells which were associated with FITC-MSM particles showed a slight shift to a lower fluorescence intensity due to the few dispersed FITC-MSM fragments internalized in Caco-2 cells. As shown in Figures 7II and 7III, these results show that cellular uptake FITC-MSNs is highly size- and concentration-dependent, respectively.

In Vitro Cytotoxicity Assay. The MSNs with different sizes and MSMs were incubated with Caco-2 cells for 24 h at various concentrations (from 10 μg/mL to 500 μg/mL), and the cytotoxicity of the particles was examined using the MTT cell viability assay. The results of MTT cell viability assay showed that the MSNs (or MSMs) used in this study were nontoxic (even at a high concentration of 500 μg/mL) (Figure 8). This result is in good agreement with those described in the literature[20,36] with similar nanoparticles. To determine which shaped particles are suitable candidates for particular applications, MSNs with different sizes and MSMs were compared for their cytotoxic effects. The cytotoxicity of MSMs was slightly higher than that of MSNs. The cytotoxicity of MSNs with sizes of about 60 nm (MSNs-2) was slightly lower than that of MSNs with sizes of about 20 nm (MSNs-1) or 90 nm (MSNs-3) at the same concentration. The toxic effect of all particles was also found to be concentration-dependent, with the higher concentrations producing the greatest toxic response.

Drug Permeability. The cultured human Caco-2 cell monolayers are generally considered representative of the intestinal epithelium as concerns drug penetration.[37,38] In all the experiments, TEER measurements showed that no cellular damage occurred. As shown in Figure 9, the transport of the drug was linear over the time period studied; both an inhibitor for P-glycoprotein (P-gp) and MSNs caused a significant increase ($P < 0.05$) in transport of TEL compared to TEL alone. The apparent permeability coefficient (P_{app}) and efflux ratio (ER) values of TEL, alone or in its combinations with an inhibitor for P-gp cyclosporin A (CsA) or MSNs, are shown in Table 1. The permeation studies elucidated the sensitivity of TEL transport to P-gp in Caco-2 cells. For the model drug TEL a higher transport from the basolateral to the apical side as compared to the reverse direction could be measured. Incubation of the cell monolayer with CsA or MSNs can reduced the efflux process of TEL in Caco-2 cell monolayers. A significant ($P < 0.05$) 2.1- and 1.7-fold increase in TEL absorption enhancement ratios (AR) was observed in systems containing CsA and MSNs, respectively. The results indicated that MSNs could significantly reduce the rate of P-gp mediated drug efflux and enhance TEL permeability.

***In Vivo* Absorption.** To further investigate the role of MSNs, the oral bioavailability of TEL-MSNs in beagle dogs was compared with that of the commercial tablet Micardis and TEL-MSMs. The mean plasma concentration versus time curves of TEL following a single dose of each formulation are shown in Figure 10, and the pharmacokinetic parameters are listed in Table 2. It can be seen that the $AUC_{0\rightarrow 72h}$ was approximately 1.29 times greater when TEL was administered as TEL-MSM tablet compared with the commercial tablet. However, the mean value of C_{max} for the TEL-MSM tablet was not significantly different from that of the commercial tablet ($p > 0.05$). It is worth noting that the TEL-MSN tablet exhibited a significantly increased $AUC_{0\rightarrow 72h}$ and C_{max} compared with the commercial tablet ($p < 0.05$). It was found that the mean value of C_{max} for the TEL-MSN tablet was approximately 1.24- and 1.13-fold greater than that of TEL administered as the commercial tablet and the TEL-MSM tablet, respectively. In addition, more rapid absorption with a t_{max} of 0.96 h was observed for the TEL-MSN tablet compared with the TEL-MSM tablet ($p < 0.05$). The significantly larger $AUC_{0\rightarrow 72h}$ obtained from the TEL-MSN tablet indicated that MSNs facilitated the fast dissolution of the drug in the gastrointestinal fluid which resulted in higher concentration gradient between the gastrointestinal lumen and blood, and enhanced drug permeability through biological membranes consequently enhanced oral bioavailability of the poorly soluble drug TEL.[39−42]

■ CONCLUSIONS

In summary, our studies support the potential value of spherical MSNs as an oral drug delivery system for poorly soluble drugs. MTT cell viability assay showed that the MSNs used in this study were nontoxic. The cellular binding, association and transport of MSNs are highly time-, concentration- and size-dependent. In addition, MSNs could significantly enhance TEL permeability and reduce rate of P-gp mediated drug efflux, and enhanced *in vivo* pharmacokinetics (increased C_{max} and bioavailability) is demonstrated for the TEL-MSN formulation when compared with either a commercial formulation or TEL-MSM formulation. A higher drug release rate and the resulting higher concentration gradient between the gastrointestinal fluids and blood as well as enhanced drug permeability through biological membranes are the principal mechanisms behind the

improved oral absorption of poorly soluble drugs promoted by MSNs. This work demonstrates the significant potential for the use of spherical MSNs as a novel delivery system for poorly soluble drugs.

AUTHOR INFORMATION

Corresponding Author

*Q.Z.: Peking University P.O. Box 90, 38 Xueyuan Road, Haidian District, Beijing, 100191, PR China; tel and fax, +86-10-82802791; e-mail, zqdodo@bjmu.edu.cn. S.W.: Shenyang Pharmaceutical University P.O. Box 32, 103 Wenhua Road, Shenhe District, Shenyang, Liaoning Province 110016, PR China; tel and fax, +86-24-23986348; e-mail, silingwang@hotmail.com.

ACKNOWLEDGMENTS

This work was supported by the National Basic Research Program of China (973 Program) (No. 2009CB930300), the National Science Foundation of China (No. 81072605) and Major National Platform for Innovative Pharmaceuticals (No. 2009ZX09301-012). We would like to thank Dr. David Jack for correcting the language.

REFERENCES

(1) Giacomini, K. M.; Huang, S. M.; Tweedie, D. J. Membrane transporters in drug development. *Nat. Rev. Drug Discovery* **2010**, *9*, 215−236.

(2) Vasconcelos, T.; Sarmento, B.; Costa, P. Solid dispersions as strategy to improve oral bioavailability of poor water soluble drugs. *Drug Discovery Today* **2007**, *12*, 1068−1075.

(3) Lipinski, C. A.; Lombardo, F.; Dominy, B. W.; Feeney, P. J. Experimental and computational approaches to estimate solubility and permeability in drug discovery and development settings. *Adv. Drug Delivery Rev.* **2001**, *46*, 3−26.

(4) White, R. E. High-throughput screening in drug metabolism and pharmacokinetic support of drug discovery. *Annu. Rev. Pharmacol.* **2000**, *40*, 133−157.

(5) Bansal, S. S.; Kaushal, A. M.; Bansal, A. K. Molecular and thermodynamic aspects of solubility advantage from solid dispersions. *Mol. Pharmaceutics* **2006**, *3*, 62−69.

(6) Ramsden, J. J. What is nanotechnology? *Nat. Nanotechnol.* **2005**, *1*, 3−17.

(7) Sahoo, S. K.; Labhasetwar, V. Nanotech approaches to drug delivery and imaging. *Drug Discovery Today* **2003**, *8*, 1112−1120.

(8) Kesisoglou, F.; Panmai, S.; Wu, Y. Nanosizing−Oral formulation development and biopharmaceutical evaluation. *Adv. Drug Delivery Rev.* **2007**, *59*, 631−644.

(9) Cruz, L. J.; Tacken, P. J.; Bonetto, F.; Buschow, S. I.; Croes, J.; Wijers, M.; Multimodal, I. Imaging of nanovaccine carriers targeted to human dendritic cells. *Mol. Pharmaceutics* **2011**, *8*, 520−531.

(10) Park, J. H.; Gu, L.; Maltzahn, G.; Ruoslahti, E.; Bhatia, S. N. Sailor M.J. Biodegradable luminescent porous silicon nanoparticles for *in vivo* applications. *Nat. Mater.* **2009**, *8*, 331−336.

(11) Pokorski, J. K.; Steinmetz, N. F. The art of engineering viral nanoparticles. *Mol. Pharmaceutics* **2011**, *8*, 29−43.

(12) Stevens, E. V.; Carpenter, A. W.; Shin, J. H.; Liu, J.; Der, C. J.; Schoenfisch, M. H. Nitric oxide-releasing silica nanoparticle inhibition of ovarian cancer cell growth. *Mol. Pharmaceutics* **2010**, *7*, 775−785.

(13) Vallet-Regi, M.; Balas, F.; Arcos, D. Mesoporous materials for drug delivery. *Angew. Chem., Int. Ed.* **2007**, *6*, 7548−7558.

(14) Barbé, C.; Bartlett, J.; Kong, L.; Finnie, K.; Lin, H. Q.; Larkin, M. Silica particles: a novel drug-delivery system. *Adv. Mater.* **2004**, *16*, 1949−1966.

(15) Mal, N. K.; Fujiwara, M.; Tanaka, Y. Photocontrolled reversible release of guest molecules from coumarin-modified mesoporous silica. *Nature* **2003**, *421*, 350−353.

(16) Slowing, I. I.; Vivero-Escoto, J. L.; Wu, C.-W.; Lin, V. S. Y. Mesoporous silica nanoparticles as controlled release drug delivery and gene transfection carriers. *Adv. Drug Delivery Rev.* **2008**, *60*, 1278−1288.

(17) Rosenholma, J. M.; Lindén, M. Towards establishing structure−activity relationships for mesoporous silica in drug delivery applications. *J. Controlled Release* **2008**, *128*, 157−164.

(18) Kilpeläinen, M.; Riikonen, J.; Vlasova, M. A.; Huotari, A.; Lehto, V. P.; Salonen, J.; Herzig, K. H.; Järvinen, K. *In vivo* delivery of a peptide, ghrelin antagonist, with mesoporous silicon microparticles. *J. Controlled Release* **2009**, *137*, 166−170.

(19) Slowing, I. I.; Trewyn, B. G.; Giri, S.; Lin, V.S.-Y. Mesoporous silica nanoparticles for drug delivery and biosensing applications. *Adv. Funct. Mater.* **2007**, *17*, 1225−1236.

(20) Wang, S. Ordered mesoporous materials for drug delivery. *Microporous Mesoporous Mater.* **2009**, *117*, 1−9.

(21) Kapoor, S.; Hegde, R.; Bhattacharyya, A. J. Influence of surface chemistry of mesoporous alumina with wide pore distribution on controlled drug release. *J. Controlled Release* **2009**, *140*, 34−39.

(22) Lia, Z. Z.; Xu, S. A.; Wen, L. X.; Liua, F.; Liu, A. Q.; Wang, Q.; Sun, H. Y.; Yu, W.; Chen, J. F. Controlled release of avermectin from porous hollow silica nanoparticles: Influence of shell thickness on loading efficiency, UV-shielding property and release. *J. Controlled Release* **2006**, *111*, 81−88.

(23) Charnay, C.; Bégu, S.; Tourné-Péteilh, C.; Nicole, L.; Lerner, D. A.; Devoisselle, J. M. Inclusion of ibuprofen in esoporous templated silica: drug loading and release property. *Eur. J. Pharm. Biopharm.* **2004**, *57*, 533−540.

(24) Salonen, J.; Laitinen, L.; Kaukonen, A. M.; Tuura, J.; Björkqvist, M.; Heikkilä, T.; Vähä-Heikkilä, K.; Hirvonen, J.; Lehto, V.-P. Mesoporous silicon microparticles for oral drug delivery: loading and release of five model drugs. *J. Controlled Release* **2005**, *108*, 362−374.

(25) Yu, H.; Zhai, Q. Z. Mesoporous SBA-15 molecular sieve as a carrier for controlled release of nimodipine. *Microporous Mesoporous Mater.* **2009**, *123*, 298−305.

(26) Thomas, M. J. K.; Slipper, I.; Walunj, A.; Jain, A.; Favretto, M. E.; Kallinteri, P.; Douroumis, D. Inclusion of poorly soluble drugs in highly ordered mesoporous silica nanoparticles. *Int. J. Pharm.* **2009**, *387*, 272−277.

(27) Mellaerts, R.; Jammaer, J. A. G.; Speybroeck, M. V.; Chen, H.; Humbeeck, J. V.; Augustijns, P.; Mooter, G. V.; Martens, J. A. Physical state of poorly water soluble therapeutic molecules loaded into SBA-15 ordered mesoporous silica carriers: a case study with itraconazole and ibuprofen. *Langmuir* **2008**, *24*, 8651−8659.

(28) Zhang, Y.; Zhang, J.; Jiang, T.; Wang, S. Inclusion of the poorly water-soluble drug simvastatin in mesocellular foam nanoparticles: Drug loading and release properties. *Int. J. Pharm.* **2011**, *410*, 118−124.

(29) Yang, P. P.; Quan, Z. W.; Lu, L. L.; Huang, S. S.; Lin, J. Luminescence functionalization of mesoporous silica with different morphologies and applications as drug delivery systems. *Biomaterials* **2008**, *29*, 692−702.

(30) Horcajada, P.; Rámila, A.; Pérez-Pariente, J.; Vallet-Regi, M. Influence of pore size of MCM-41 matrices on drug delivery rate. *Microporous Mesoporous Mater.* **2004**, *68*, 105−109.

(31) Zhang, Y.; Zhi, Z.; Jiang, T.; Zhang, J.; Wang, Z.; Wang, S. Spherical mesoporous silica nanoparticles for loading and release of the poorly water-soluble drug telmisartan. *J. Controlled Release* **2010**, *145*, 257−263.

(32) Zhao, D. Y.; Feng, J. L.; Huo, Q. S.; Melosh, N.; Fredrickson, G. H.; Chmelka, B. F.; Stucky, G. D. Triblock copolymer syntheses of mesoporous silica with periodic 50 to 300 angstrom pores. *Science* **1998**, *279*, 548−552.

(33) Tran, P. H. L.; Tran, H. T. T.; Lee, B. J. Modulation of microenvironmental pH and crystallinity of ionizable telmisartan using alkalizers in solid dispersions for controlled release. *J. Controlled Release* **2008**, *129*, 59−65.

(34) Nan, A. J.; Bai, X.; Son, S. J.; Lee, S. B.; Ghandehari, H. Cellular uptake and cytotoxicity of silica nanotubes. *Nano Lett.* **2008**, *8*, 2150−2154.
(35) Zhao, Y. N.; Sun, X. X.; Zhang, N.; Trewyn, B. G.; Slowing, I. I.; Lin, V. S. Y. Interaction of mesoporous silica nanoparticles with human red blood cell membranes: size and surface. *ACS Nano* **2011**, *5*, 1366−1375.
(36) He, Q.; Shi, J.; Chen, F.; Zhu, M.; Zhang, L. An anticancer drug delivery system based on surfactant-templated mesoporous silica nanoparticles. *Biomaterials* **2010**, *31*, 3335−3346.
(37) Zhang, L.; Strong, J. M.; Qiu, W.; Lesko, L. J.; Huang, S. M. Scientific perspectives on drug transporters and their role in drug interactionst. *Mol. Pharmaceutics* **2006**, *3*, 62−69.
(38) Leslie, Z. B. The drug transporter−metabolism alliance: uncovering and defining the interplay. *Mol. Pharmaceutics* **2009**, *6*, 1631−1643.
(39) Meng, H.; Liong, M.; Xia, T.; Li, Z.; Ji, Z.; Zink, J. I.; Nel, A. E. Engineered design of mesoporous silica nanoparticles to deliver doxorubicin and P-Glycoprotein siRNA to overcome drug resistance in a cancer cell line. *ACS Nano* **2010**, *4*, 4539−4550.
(40) Amidon, G. E. Oral bioperformance and 21st century dissolution. *Mol. Pharmaceutics* **2010**, *7*, 1361−1361.
(41) Thommes, M.; Ely, D. R.; Carvajal, M. T.; Pinal, R. Improvement of the dissolution rate of poorly soluble drugs by solid crystal suspensions. *Mol. Pharmaceutics* **2011**, *8*, 727−735, DOI: 10.1021/mp1003493.
(42) Richard, B. K. Transporters and drug discovery: Why, When, and How. *Mol. Pharmaceutics* **2006**, *3*, 26−32.